International Journal of Automotive Technology, Vol. 13, No. 4, pp. 541−552 (2012)
DOI 10.1007/s12239−012−0052−1

pISSN 1229−9138/ eISSN 1976-3832

NON-LINEAR DYNAMIC SIMULATION OF GEAR RESPONSE UNDER THE IDLING CONDITION

Z. G. CHEN[1], Y. M. SHAO[1)*] and T. C. LIM[2)]

[1)]State Key Laboratory of Mechanical Transmission, Chongqing University, Chongqing 400030, China
[2)]School of Dynamic Systems, Mechanical Engineering, University of Cincinnati, Cincinnati, OH 45221-0072, USA

(Received 7 February 2011; Revised 27 July 2011; Accepted 8 November 2011)

ABSTRACT−A dynamic lumped-parameter gear model incorporating the effects of a time-varying and asymmetric mesh stiffness and a backlash nonlinearity is formulated to analyze the spur gear rattle response under the idling condition. The proposed theory assumes a rectangular time-varying mesh stiffness function. The phase shift between the mesh stiffness for forward and backward contacts is examined. Numerical studies are employed to examine the effects of engine torque fluctuations and tooth surface friction on the gear rattle response and the corresponding tooth impact behavior. Comparisons between the results from the time-invariant mesh stiffness model and the proposed time-varying mesh stiffness model reveal differences in the gear responses, especially when the mean rotational speed of the fluctuating gear pair is non-zero. The analysis reveals significant effects on the high frequency response components. However, the idling gear dynamics are relatively insensitive to tooth surface friction.

KEY WORDS : Idling gear, Backlash, Non-linear gear dynamics, Time-varying mesh stiffness, Gear rattle, Phase shift

NOMENCLATURE

T_p/T_g : external and braking torques
Ω_p/Ω_g : nominal operational speeds of pinion and gear
θ_a : angular position of the tooth of pinion as it just moves into meshing zone
θ_c : angular position of another tooth of pinion corresponding to θ_a
θ_d : angular position of the tooth of pinion when it just left meshing
θ_b : angular position of another tooth of pinion corresponding to θ_d
θ_p : angular position of the tooth of pinion when gear teeth contacts at pitch point
$\theta_A/\theta_C/\theta_D/\theta_B/\theta_p$: only for the backward tooth contact in Figure 1(b)
$\theta_a/\theta_c/\theta_d/\theta_b/\theta_p$: only for forward tooth contact in Figure 1(a)
LOA : line of action
OLOA : off line of action
K_m/C_m : meshing stiffness and damping coefficient
K_d/K_s : mesh stiffness for double-tooth and single-tooth engagement respectively
$\xi(t)$: dynamic transmission error
η : one-half of the backlash of the gear teeth flank
$e(t)$: transmission error function
R_{ij} : radius, subscript $i - p$, g for pinion and gear respectively, j−a, p ,b for addendum, pitch and base circles respectively
z_p/z_g : number of teeth of pinion/gear
J_p/J_g : inertial moment of pinion/gear
m_p/m_g : mass of pinion/gear
λ : distance of the two adjacent teeth of pinion along the LOA
$\theta_p(t)$: rotating angle of pinion normalized by λ divided by R_{pb}
α : pressure angle on pitch line
θ_0 : illustrated in Figure 1(a)
F_k/F_c : elastic force/dissipative force
ε : manufacturing errors on the tooth
Δ : contact-type coefficient
$y_p,\dot{y}_p,\ddot{y}_p/y_g,\dot{y}_g,\ddot{y}_g$: lateral displacement, velocity, acceleration of pinion/gear along LOA
$x_p,\dot{x}_p,\ddot{x}_p/x_g,\dot{x}_g,\ddot{x}_g$: lateral displacement, velocity, acceleration of pinion/gear along OLOA
K_{pBx}/K_{gBx} : stiffness of the supporting bearing of pinion/ gear along OLOA
C_{pBx}/C_{gBx} : damping of the supporting bearing of pinion/ gear along OLOA
K_{pBy}/K_{gBy} : stiffness of the supporting bearing of pinion/ gear along LOA
C_{pBy}/C_{gBy} : damping of the supporting bearing of pinion/ gear along LOA
θ_p/θ_g : angular displacement of pinion/gear
$\dot{\theta}_p/\dot{\theta}_g$: angular velocity of pinion/gear
$\ddot{\theta}_p/\ddot{\theta}_g$: angular acceleration of pinion/gear

*Corresponding author. e-mail: ymshao@cqu.edu.cn

F_f/M_f : friction force/moment
N : contact force
C_g : damping between gear and shaft due to lubrication
Γ : profile contact ratio of gears
A : amplitude of angular acceleration
f_e : frequency of angular acceleration
u : friction coefficient
v : rotational speed of pinion
σ : contact ratio

1. INTRODUCTION

Gear rattle and the tooth impacts caused by input and output torque fluctuations under idling or lightly loaded conditions are often caused by the presence of gear backlash. This dynamic behavior can increase the noise in the vehicle interior. As the demand for quieter vehicle interiors continues to grow, car manufacturers are becoming more concerned about acoustic noise problems, especially from the noise generated by gearboxes (Dion *et al*., 2009; Dogan, 1999; Heinrichs and Bodden, 1999). Gear rattle is a source of gearbox noise that often annoys passengers. The existence of gear rattle in power transmission systems and its impact on the automotive industry has been widely reported in the literature (Wang *et al*., 2002; Kim *et al*., 2008; Yakoub *et al*., 2004; Han *et al*., 2009; Luo and O'Connor, 2011; Shim *et al*., 2011). Idle gear rattle is associated with the generation and radiation of a characteristic impulsive noise from the impact of mating gear teeth (Dion *et al*., 2009; Tangasawi *et al*., 2007). The noise is primarily attributed to the torsional vibration of the crankshaft due to excitations from the engine ring and from inertial forces (Shih *et al*., 2001; Wang *et al*., 2001; Fujimoto *et al*., 1987). These excitations cause fluctuating angular responses of the shafts in the transmission system, which then create the tendency for the gears to oscillate within their backlash, resulting in the mating gear teeth colliding with each other (Tangasawi *et al*., 2007; Padmanabhan *et al*., 1995). The impulsive nature of gear rattle noise tends to make it more annoying than most other responses from the powertrain system. In fact, the gear rattle response possesses a distinct sound quality that differentiates it from the acoustic noise produced by other mechanisms in the vehicle. Furthermore, with the continual improvement in vehicle design resulting in lower interior noise from the engine and other sources, the gear rattle problem is even more noticeable when it occurs (Wang *et al*., 2001; Theodossiades *et al*., 2007). Consequently, the problem has been frequently studied. Some of the relevant studies are discussed here.

Sarkar *et al*. (1997) presented a study that used modeling, simulation and experimentation to detect the degree of backlash in geared mechanisms and suggested that the proposed approach could be applied to understanding gear dynamics and faults. Han *et al*. (2009) developed a new multi-body dynamic model to predict the mesh force during gear rattle. Russo *et al*. (2009) performed a series of experiments to quantify the effect of lubrication on the idle gear rattle response of helical pairs inside an automotive gearbox. Their results show good agreement with the predictions of a single-degree-of-freedom theoretical model that accounts for the oil squeeze effect between the gear teeth during the non-contact phases. However, the difference in the mesh stiffness for forward and backward contact was not considered in their studies. Crowther *et al*. (2007) analytically, computationally and experimentally studied the gear tooth impact responses of an automatic transmission system with multiple clearances. They show that the impacts within the planetary and differential gears may occur under combinations of engine, braking and vehicle transient loads. However, the mesh stiffness used in their study is assumed to be constant. Walha *et al*. (2009) investigated the dynamics of a two-stage geared rotor system involving backlash and time-dependent mesh stiffness. Brauer (2005) reported a theoretical analysis of transmission errors in gearboxes containing an anti-backlash conical involute design intended to reduce or eliminate the unwanted backlash in mechatronic products. In the analytical studies of the dynamics of gear rattle and tooth impacts under idling or lightly loaded conditions, there are two frequently applied modeling assumptions about the gear mesh stiffness. In one group of models, the mesh stiffness is assumed to be time-invariant (Dion *et al*., 2009; Kim and singh, 2001), whereas the other group uses a time-varying mesh stiffness formulation (Wang *et al*., 2002; Yakoub *et al*., 2004). Furthermore, the gear mesh stiffness value is often assumed to be symmetric, which means that the phase shift between the mesh stiffness for the forward and the backward tooth contacts is ignored in these models. In the present paper, a time-varying mesh stiffness including the effect of the phase shift between the forward and the backward tooth contacts is used, and the simulation results show that previously unobserved dynamic responses can be studied with this more realistic gear mesh stiffness model.

Numerous approaches have been employed to determine the mesh stiffness used in dynamic gear models. The finite element model (FEM) is one of the most widely employed tools. However, this approach tends to be computationally intensive, especially when the number of elements in the gear tooth model is substantial (Wu *et al*., 2008; Pimsarn and Kazerounian, 2002; Wang, 2003). Analytical and semi-analytical models are usually more efficient than FEM, and in some cases they may yield satisfactory tooth mesh stiffness results (Chaari *et al*., 2009; Weber, 1949; Cornell, 1981; Houser and Harianto, 1998; Houser *et al*., 2004). Brancati *et al*. (2005), Umezawa *et al*. (1986) and Cai

(1995) have used approximate theories to model the gear mesh stiffness as a function of the position of the pinion in the contact zone, the tooth width, the tooth depth and the helix angle. In the analysis in this paper, a time-varying rectangular-form mesh stiffness function is used whose values for double-tooth and single-tooth engagement are based on the finite element work of Wu *et al*. (2008).

To address the gap in the literature, the present study assumes the mesh stiffness to be time-varying and dissimilar between the forward and backward tooth contacts, even at the same pinion angular position. As noted above, this improved mesh stiffness model has not been considered in past investigations, and it is shown here to have a significant influence on the dynamic response of the geared rotor system. The present work focuses on analyzing the dynamic response of a spur gear pair under the idling condition. The proposed model adopts a gear impact theory based on the work of Dion *at al*. (2009) and uses lumped stiffness and damping representations to model the supporting bearings. The resulting dynamic lumped-parameter gear model is a coupled lateral-torsional vibrating system with six degrees of freedom (DOF). The unique contributions of this paper to the study of gear rattle dynamics are the formulation and analysis of a time-varying mesh stiffness model that integrates the phase-shift effect of forward and backward tooth contacts and the dynamic interactions of the bearing supports and the gear rattle. It is expected that the more realistic mesh stiffness representation will result in more accurate predictions of dynamic responses and a better understanding of the gear rattle phenomenon.

The paper is organized as follows. The section 1 introduces the previous relevant studies, describes the proposed problem and explains the main objective of this study. Next, the lumped-parameter dynamic model of the idling spur gear system, including forward and backward tooth contact, is formulated in section 2. The resultant model is used in numerical simulations, and the corresponding parametric analysis of the results is examined in detail in section 3. Finally, some conclusions will be drawn in section 4.

2. FORMULATION OF IDLE GEAR DYNAMICS

2.1. Mesh Stiffness Model

Figure 1 shows the two tooth-contact geometries considered in this study, namely forward and backward tooth contacts. In this schematic, the critical points are labeled as **a**, **b**, **p**, **c** and **d** for the forward tooth contact and **A**, **B**, **P**, **C** and **D** for the backward tooth contact. In the forward tooth contact geometry, the position **a** is the contact point where a tooth pair just enters the mesh zone; a second tooth pair simultaneously contacts at position **c**. When the second tooth pair is about to exit the meshing zone at position **d**, the first pair is making contact at position **b**. The position **p** is the pitch point where the tooth surface friction force changes its direction. The same definitions can be applied to the backward contact case, corresponding to positions **A**, **B**, **C**, **D** and **P** in Figure 1(b).

Two types of forward and backward oscillatory impact behaviors of a meshing spur gear pair are shown in Figure 2. The gear denoted by the black solid curve represents forward contact, and the dotted curve represents backward contact. The letters **a**, **b**, **A** and **B** refer to contact points. One type of oscillatory impact involves double-tooth contact for both forward (points **a** and **b**) and backward (points **A** and **B**) oscillations as shown in Figure 2(a). The other type of impact causes double-tooth contact in one direction (points **a** and **b**) and single-tooth contact in the opposite direction (point **A**) as shown in Figure 2(b). Note that a third type of impact behavior, in which single-tooth contacts occur in both directions, is not shown here for brevity.

The phase relationship for the forward and backward contacts is also shown in Figure 2(b). Here, $\theta_p(t)$ is the rotational angle and O_p is the geometric center of the pinion. The positions where the gear pair contacts at point **a** for forward contact in Figure 1(a) and point **A** for backward contact in Figure 1(b) are chosen to be the origins of the mesh stiffness curves in this paper. Thus, in Figure 2(b), the magnitudes of the mesh stiffness are dependent on the angle $\theta(t)= \theta_p(t)=\angle BO_pD-\theta_0$ for forward contact and $\theta(t)=\angle EO_pC-\theta_0$ for backward contact. The pinion rotational angle θ_0 shown in Figure 1a is the

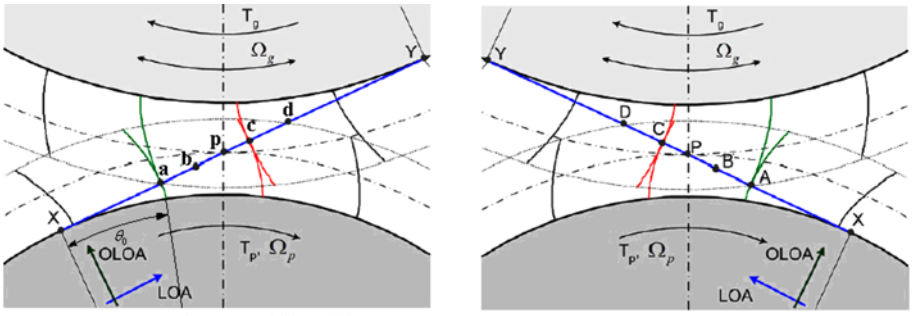

(a) Forward contact (drive side) (b) Backward contact (coast side)

Figure 1. Gear tooth meshing process with OLOA (off line of action) and LOA (line of action).

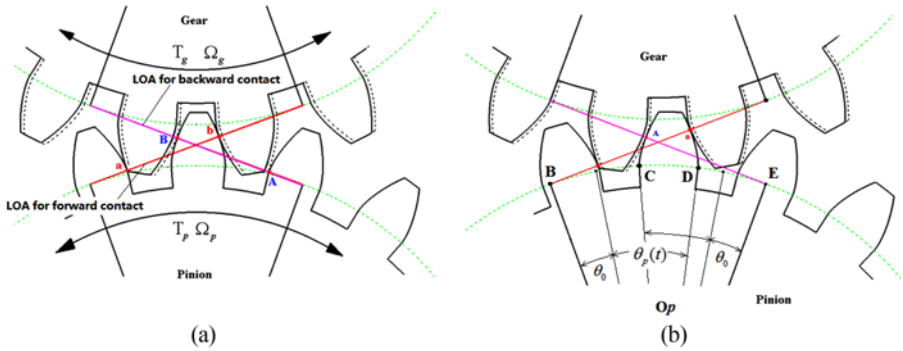

Figure 2. Oscillatory impacts of a gear pair (**a**, **b** - forward rotation contact points; **A**, **B** - backward rotation contact points) when (a) double-tooth contact occurs in both directions and (b) both single-tooth and double-tooth contacts are present.

rotational angle between the position of the pinion where a tooth is just rotating into the LOA (point X) and the position where it just engages with its mating tooth at contact point **a**. θ_0 can be calculated using Equation (1):

$$\theta_0 = \frac{(R_{pp}+R_{gp})\sin\alpha - \sqrt{R_{ga}^2 - R_{gb}^2}}{R_{pb}}. \quad (1)$$

As described above, the mesh stiffness values corresponding to the same pinion angular position are different in the forward (drive side) and backward (coast side) tooth contact conditions. This phenomenon gives rise to asymmetry in the mesh stiffness function. In the case of a spur gear pair, the asymmetry can be clearly seen in the example shown in Figure 3, where the gear mesh stiffness is plotted as a function of the pinion angular position for both the forward and backward tooth contacts. Note that the two sets of subscripts **a**, **b**, **p**, **c** and **d** and **A**, **B**, **P**, **C** and **D** used in Figure 3 correspond to the physical contact points for the forward and backward gear rotations as shown in Figure 1.

In the forward rotation case, θ_a is the pinion angular position at which the tooth enters into engagement and θ_d is the angular position where the tooth pair disengages. In the regions of θ_a-θ_b and θ_c-θ_d, there are two pairs of teeth in mesh. However, only a single gear tooth pair is in contact in the θ_b-θ_c region. θ_p is the pinion angular position at which the gear tooth pair in contact is at the pitch point. When the gear pair rotates in the reverse direction, the corresponding regions are denoted by θ_A, θ_B, θ_C, θ_D and θ_P. When the two rotational cases are plotted simultaneously as a function of the pinion angular position, as shown in Figure 3 based on the definitions used in Figure 2, a phase differential between the forward and the backward gear rotations can be clearly seen. This phase shift results in two types of contact behavior, producing different gear mesh stiffness on the drive and coast sides for a given pinion angular position.

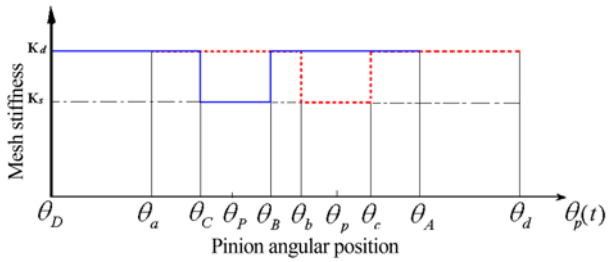

Figure 3. Mesh stiffness variations within a gear meshing cycle for both forward and backward tooth contacts. (Keys: K_d, K_s- mesh stiffness for double-tooth and single-tooth engagements; ▬ ▬ ▬, ——: mesh stiffness curves for forward and backward tooth contacts).

Taking into account the different contact behavior of the gear pair in forward and backward rotation, the position-dependent mesh stiffness for the gear pair can be written as,

$$K_m = K(\theta(t), \xi(t), \eta, e(t)). \quad (2)$$

On the drive side, when the teeth are in contact,

$$\xi(t) > e(t) + \eta, K_m = K(\theta(t)), \theta(t) = \theta_p(t). \quad (3a,b,c)$$

When the teeth disengage,

$$|\xi(t)| < e(t) + \eta, K_m = 0. \quad (4a,b)$$

According to the angular relationship in Figure 2b,

$$\angle BO_pD + \angle EO_pC - \angle CO_pD = \angle BO_pE, \quad (5)$$

where

$$\angle BO_pD = \theta_0 + \theta_p(t), \angle CO_pD = \frac{\pi}{z_p} + 2(\tan\alpha - \alpha), \angle BO_pE = 2\alpha. \quad (6a,b,c)$$

The relationship between the phase angle θ(t) and the pinion angular position θ_p(t) can be obtained by the substitution of (6) into (5) as shown as equation (7c). Thus, for the coast side, when the teeth are in contact,

$$\xi(t)<-(e(t)+\eta), K_m=K(\theta(t)), \theta(t)=\frac{\pi}{z_p}+2\tan\alpha-2\theta_0-\theta_p(t), \quad (7a,b,c)$$

where K_m is the mesh stiffness; $e(t)$ is the transmission error function, which is not of interest in this analysis and is assumed to be zero; η is one-half of the backlash; z_p is the number of pinion teeth; α is the pressure angle at the pitch line; and $\theta_p(t)$ is the pinion angular position.

2.2. Mesh Force Calculations

The formulation of the contact force computation is partly based on the theory proposed by Dion *et al*. (2009). Here, the constant stiffness used in their model is substituted with the proposed time-varying mesh stiffness representation with the dissimilar effects of the forward and backward gear rotations as described above. Considering these effects, the explicit expressions for the elastic force F_k and the dissipative force F_c are as follows:

$$F_k=K_m(\xi-\eta)\left|\frac{\xi-\eta}{2\eta}\right|^{\Delta-1}, F_c=C_m\xi \text{ for } \xi\geq\eta+\varepsilon, \quad (8a,b)$$

$$F_k=\frac{K_m}{2}\left(1-\left(\frac{\varepsilon}{2}+\zeta-\eta\right)\sin\left(\frac{\pi}{\varepsilon}\right)\right)(\xi-\eta)\left|\frac{\xi-\eta}{2\eta}\right|^{\Delta-1}, \quad (9a)$$

$$F_c=\frac{C_m}{2}\left(1-\left(\frac{\varepsilon}{2}+\xi-\eta\right)sin\left(\frac{\pi}{\varepsilon}\right)\right)\xi \text{ for } \eta\leq\xi\leq\eta+\varepsilon, \quad (9b)$$

$$F_k=0, F_c=0 \text{ for } -\eta\leq\xi\leq\eta, \quad (10a,b)$$

$$F_k=\frac{K_m}{2}\left(1-\left(\frac{\varepsilon}{2}+\xi+\eta\right)\sin\left(\frac{\pi}{\varepsilon}\right)\right)(\xi+\eta)\left|\frac{\xi+\eta}{2\eta}\right|^{\Delta-1}, \quad (11a)$$

$$F_k=\frac{C_m}{2}\left(1-\left(\frac{\varepsilon}{2}+\xi+\eta\right)\sin\left(\frac{\pi}{\varepsilon}\right)\right)\xi \text{ for } -\eta-\varepsilon\leq\xi\leq-\eta, \quad (11b)$$

$$F_k=K_m(\xi+\eta)\left|\frac{\xi+\eta}{2\eta}\right|^{\Delta-1}, F_c=C_m\dot{\xi} \text{ for } \xi\leq-\eta-\varepsilon, \quad (12a,b)$$

where ε is a measure of the manufacturing errors on the tooth (such as shape defects and micro-geometric deformities) and K_m is the static stiffness of the contact between the meshing gear teeth, which can be obtained from finite element methods. Note that the effect of tooth bending is included in K_m. C_m is the damping of the contact between the meshing teeth; Δ is the contact-type coefficient (3/2 for a point-contact model and 10/9 for line contact); and ξ is the dynamic transmission error (DTE) which can be computed from

$$\xi=\theta_pR_{pb}-\theta_gR_{gb}+y_p-y_g \quad (13)$$

where θ_p and θ_g are the angular displacements of the pinion and the gear and y_p and y_g are the lateral displacements of the pinion and the gear along the LOA. A more detailed discussion of the parameters can be found in Dion *et al*. (2009). Note that the effects of the support bearings and the shafts are implicitly included in the above equation as the lateral restraints on the pinion and the gear (Fujimoto and Kizuka, 2001). Additionally, the vibrations transmitted through the bearings excite the housing structure, which in turn radiates acoustic noise (Wang *et al*., 2001).

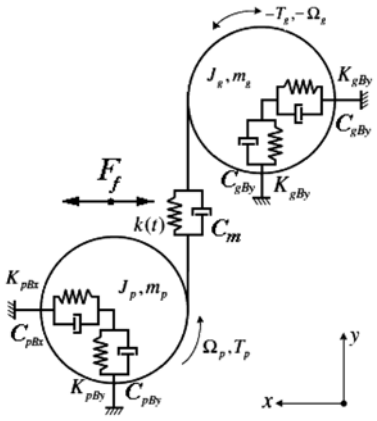

Figure 4. Spur gear pair system having six degrees of freedom.

2.3. Spur Gear Pair System

Using the proposed mesh stiffness and enhanced mesh force formulations, a dynamic lumped-parameter model is developed for a spur gearbox system in the idling condition comprising six degrees of freedom. A schematic of the dynamic gear model is shown in Figure 4. The system equations of dynamic motion are derived here.

The equations of motion governing torsional vibration are represented by

$$J\ddot{\theta}=T \quad (14a)$$

$$J=\begin{bmatrix}J_p & 0\\ 0 & J_g\end{bmatrix}, \theta=\begin{bmatrix}\theta_p\\ \theta_g\end{bmatrix}, T=\begin{bmatrix}T_p-M_{pN}+M_{pf}\\ -T_g+M_{gN}-M_{gf}-C_g\dot{\theta}_g\end{bmatrix}. \quad (14b)$$

The equations of motion describing the translational vibration are as follows:

$$M\ddot{X}=F, \quad (15a)$$

$$M=\begin{bmatrix}m_p & & & \\ & m_g & & \\ & & m_p & \\ & & & m_g\end{bmatrix}, X=\begin{bmatrix}x_p\\ x_g\\ y_p\\ y_g\end{bmatrix}, \quad (15b)$$

$$F=\begin{bmatrix}F_f-K_{pBx}x_p & -C_{pBx} & \dot{x}_p\\ -F_f-K_{pBx} & x_g-C_{gBx}\dot{x}_g\\ -N-K_{pBy} & y_p-C_{pBy}\dot{y}_p\\ N-K_{gBy}y_g & -C_{pBy} & \dot{y}_g\end{bmatrix}, \text{ for drive-side contact} \quad (15c)$$

Table 1. Design parameters of the spur gear system analyzed.

Parameters	Pinion	Gear
Module (mm)	2	
Pressure angle (degrees)	20	
Contact ratio	1.6456	
Number of teeth	19	48
Mass moment of inertia (kg·m^2)	4.3659×10^{-4}	8.3602×10^{-3}
Mass (kg)	0.96	2.88
Bearing radial stiffness (N/m)	6.56×10^{7}	6.56×10^{7}
Bearing damping coefficient (Ns/m)	1.8×10^{5}	1.8×10^{5}
Gear mesh stiffness (N/m)	$K_{max}=10.3\times10^{8}$, $K_{min}=6.2\times10^{8}$	
Damping of gear teeth (N·s/m)	67	
Damping of gear-shaft interface (N·m·s/rad)	0.025	
Backlash (μm)	40	
Coefficient of Friction	0.06	

$$F=\begin{bmatrix}-F_f\cos(2\alpha)+N\sin(2\alpha)-K_{pBx}x_p-C_{pBx}\dot{x}_p\\ F_f\cos(2\alpha)-N\sin(2\alpha)-K_{gBx}x_g-C_{gBx}\dot{x}_g\\ F_f\sin(2\alpha)+N\cos(2\alpha)-K_{pBy}x_p-C_{pBy}\dot{y}_p\\ -F_f\sin(2\alpha)-N\cos(2\alpha)-K_{gBy}x_g-C_{gBy}\dot{y}_g\end{bmatrix}, \text{ for coast-side contact} \quad (15d)$$

Here, N is the net contact force due to the elastic and dissipative forces presented earlier. Additionally, F_f is the tooth friction force caused by the sliding between the mating teeth. Note that all symbols are also defined in the appendix.

3. SIMULATION RESULTS

The simulation is programmed in Matlab (The MathWorks, Inc., Natick, Massachusetts, USA) with the ODE45 subroutine. In this section, the design parameters and the results of the simulation of the dynamic responses for various excitation frequencies and tooth surface friction coefficients are presented.

3.1. Design Parameters

The design parameters for the spur gear system used in this study are shown in Table 1. The mesh stiffness K, a key parameter in gear dynamics, can be obtained by numerical identification from a finite element model of teeth in contact (Howard *et al*., 2001) or, more easily, by the use of analytical models (Wu *et. al*, 2008; Chaari *et al*., 2009). The Coulomb friction model and the dynamic coefficient of friction u measured by Rebbechi *et al*. (1996) are used in this paper. Figure 5 shows the friction coefficient versus the pinion angular position over the entire zone of engagement. The calculations of the forces and the moments resulting

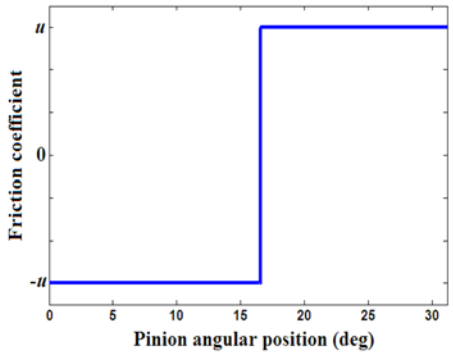

Figure 5. Coulomb friction model.

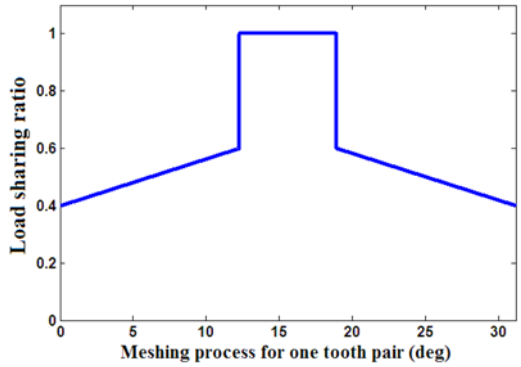

Figure 6. Load sharing ratio versus rotational angle of pinion.

from the friction on the gear teeth surfaces used in this paper are based on the method proposed by He *et al*. (2008). The load sharing ratio used in this study to calculate the friction moments, shown in Figure 6 over one tooth mesh cycle, is derived from the study by Howard *et al*. (2001) based on the finite element model (FEM) proposed by Sirichai (1999).

The value of ε =1.0 micron suggested by Dion *et al*. (2009) is used in the calculations here. Additionally, the value of the contact-type coefficient Δ is taken to be 4/3 as suggested by Dion *et al*. (2009). For comparison with the proposed time-varying mesh stiffness model, a time-invariant model with constant mesh stiffness, which has been validated by Dion *et al*. (2009) experimentally, is also analyzed in a manner similar to Vaishya and Singh (2001). The equation for the constant mesh stiffness of both the single-tooth and double-tooth engagements is

$$K_{mean}=K_d(\Gamma-1)+K_s(2-\Gamma), \quad (16)$$

where K_d is the mesh stiffness for the double-tooth engagement, K_s is the stiffness for the single-tooth condition and Γ is the profile contact ratio of the gears.

Using the resultant formulation for the spur gear system

response under the idling condition, a series of numerical simulations using the design parameters in Table 1 for both the time-invariant and the time-varying mesh stiffness representations is performed. The aim of the calculations is to quantify the effects of engine torque fluctuations and tooth surface friction on the gear dynamics. It may be noted that three sets of related experiments were conducted for input shaft excitation frequencies between 30-60 Hz by Dion *et al*. (2009). In the numerical analysis, an acceleration excitation is imposed on the pinion to simulate the operating speed fluctuation, which is defined as

$$\ddot{\theta}_p = A\sin(2\pi f_e t), \tag{17}$$

where A and f_e are the amplitude and the frequency of the angular acceleration excitation, respectively.

3.2. Dynamic Response under the Idling Condition

The DTE response under the idling operating condition is computed using Equation (13) for both the time-invariant and the time-varying mesh stiffness cases. The time history and frequency response results for pinion rotational speeds of 0 and 1000 rpm are shown in Figure 7. The same characteristics observed in the experimental and numerical studies on idle gear dynamics (Dion *et al*., 2009) can be observed here. Specifically, the results reveal that impact occurs several times on the same tooth contact side (known as single-sided tooth impact) before switching over to the other side (i.e., double-sided tooth impact). This is because the first impact is not strong enough to propel the tooth to the other side, and two or more impacts are required for the contact side to switch. From the results, it can be seen that when the pinion mean rotational speed is zero as shown in

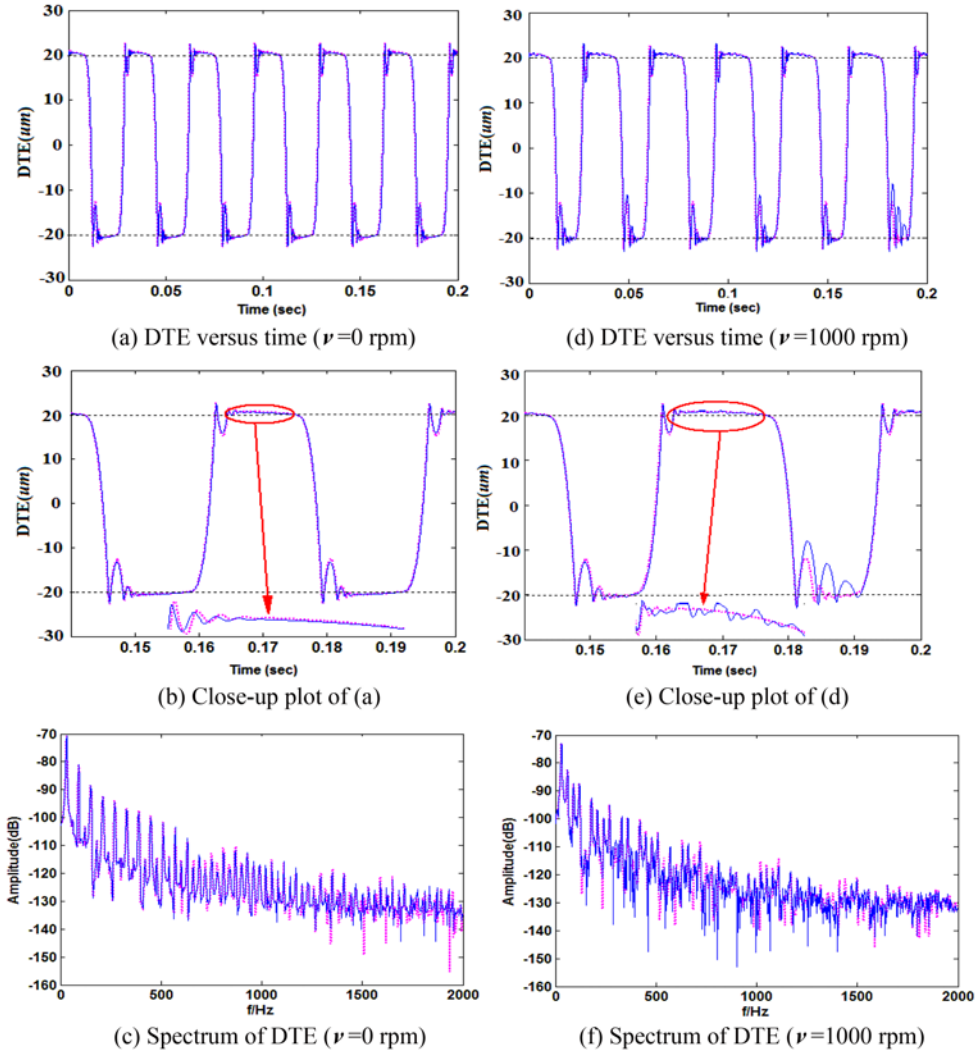

Figure 7. DTE response (A=1000 rad/s^2, f_e=30 Hz, u=0).
(Keys: ····· time-invariant mesh stiffness response, ——— time-varying mesh stiffness response, ····· upper and lower limits of idling gear free motion).

Figure 7(a)-(c), the time-invariant (mauve dashed curves) and the time-varying (blue solid curves) mesh stiffness models predict nearly the same gear responses under the idling condition. The DTE time response in Figure 7(a)-(b) and the frequency spectrum in Figure 7(c) show very little difference between the gear responses of the two cases except in the higher frequency range. Additionally, the plots clearly show that the time domain response of the vibrating gear pair reaches the boundaries of the free motion, which confirms the existence of single-sided and double-sided tooth impacts.

In contrast, when the pinion rotational speed is 1000 rpm, a distinct higher frequency fluctuation (mauve dashed curves) due to the change in the mesh stiffness is observed that is not seen in the time-invariant mesh stiffness case, as shown in Figure 7(d)-(e). This characteristic fluctuation is clearly seen in the close-up view of the DTE time-history curve in Figure 7(e) in the time interval from 0.164 to 0.175 second.

The shapes of the DTE curves in Figure 7(a)-(b) appear to be nearly symmetrical for forward and backward tooth contacts, and the proportion of the contact time is about the same for forward and backward tooth contacts. Furthermore, the number of tooth impacts in the forward and backward contact conditions is nearly the same. However, when the mean rotational speed of the pinion is not zero, as shown in Figure 7(d)-(e), the tooth impact time is shorter and there are fewer impacts for backward contact.

In the response spectra shown in Figure 7(c)-(f), the high frequency (>600 Hz) response for the time-varying mesh stiffness case is quite different from the response for the time-invariant mesh stiffness case. Furthermore, compared to the case when the rotational speed is 0 rpm shown in Figure 7(c), when a constant pinion rotational speed of

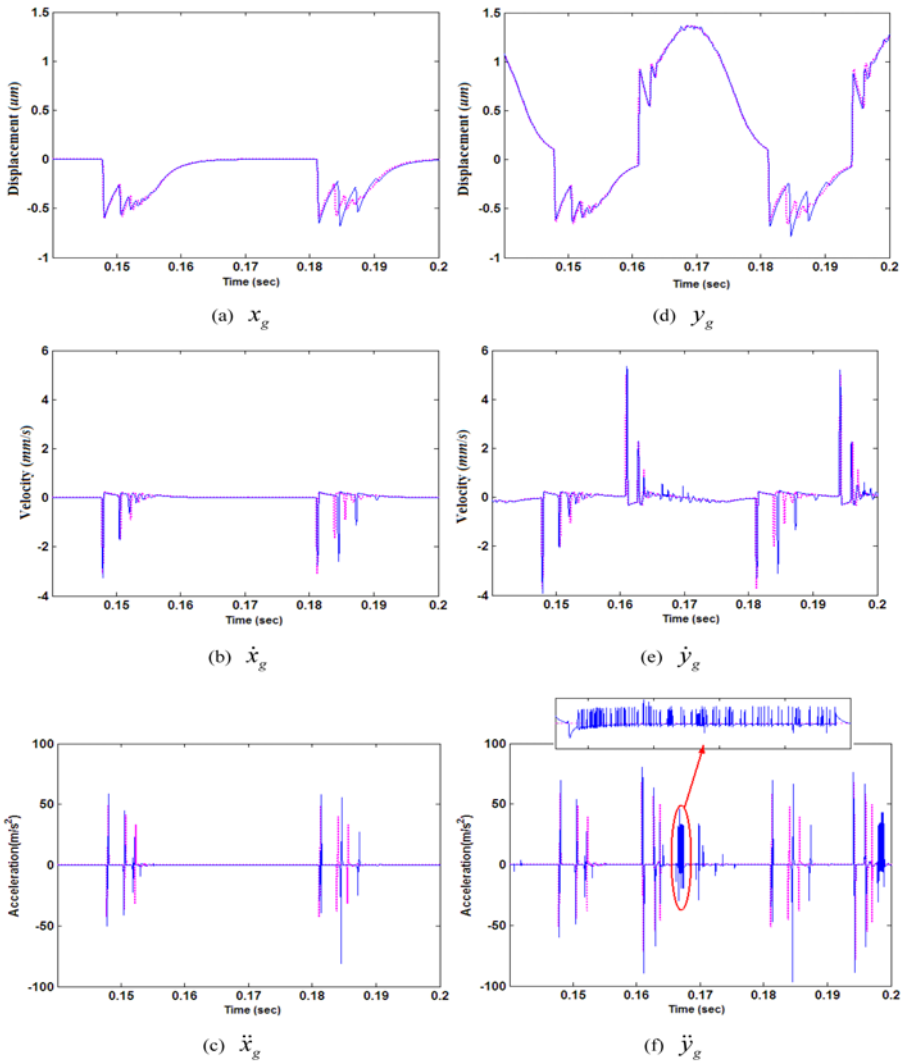

Figure 8. Lateral vibration response of gear (A=1000 rad/s^2, f_e=30 Hz, v=1000 rpm, u=0).
(Keys: ····· time-invariant meshing stiffness model, ——— time-varying mesh stiffness model developed in section 2.1).

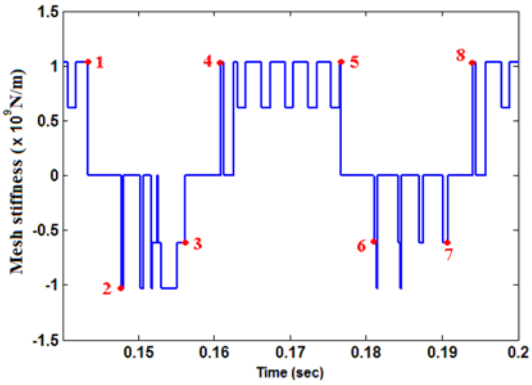

Figure 9. Mesh stiffness versus time corresponding to the results in Figure 8.

1000 rpm is applied, the DTE spectral response shown in Figure 7(f) reveals many more frequencies for the time-invariant mesh stiffness.

The corresponding lateral vibrations of the gear in the ***x*** and ***y*** directions for the same conditions shown in Figure 7 with a pinion rotational speed of 1000 rpm are illustrated in Figure 8. In the absence of tooth sliding friction, the vibrations in the ***x*** direction are caused only by the backward tooth contact, but the responses in the ***y*** direction are affected by both the forward and backward tooth contacts. Additionally, the analysis shows that the time-varying mesh stiffness affects the amplitudes and the time intervals of the gear lateral impact vibrations. The high frequency vibrations shown in Figure 8(f) are also obtained only with the time-varying mesh stiffness model. These vibrations are not observed in the time-invariant mesh stiffness case (mauve dashed curve). In all cases analyzed, the phase shift from the time-varying mesh stiffness for the forward and backward contacts produces quite different torsional and lateral dynamic responses than the time-invariant stiffness.

The alternation between double-tooth and single-tooth engagements is manifested in the mesh stiffness curve in Figure 9. In the figure, the red integer labels from 1 to 8 denote the mesh stiffness just before and just after the contact switches from one side to the other side. The difference between the mesh stiffness for the forward and the backward tooth contacts is believed to be caused by the phase shift, which makes the mesh stiffness appear asymmetric as shown in Figure 3.

From another case study, using the same conditions as in Figure 7 except that the input shaft excitation frequency is changed from 30 to 60 Hz, the DTE and its spectrum are shown in Figures 10 and 11, respectively. The differences between the responses predicted by the proposed time-varying mesh stiffness model and the previous time-invariant model can be observed in both the time and frequency domains. At low frequencies (<300 Hz), only slight differences can be seen. However, the differences are

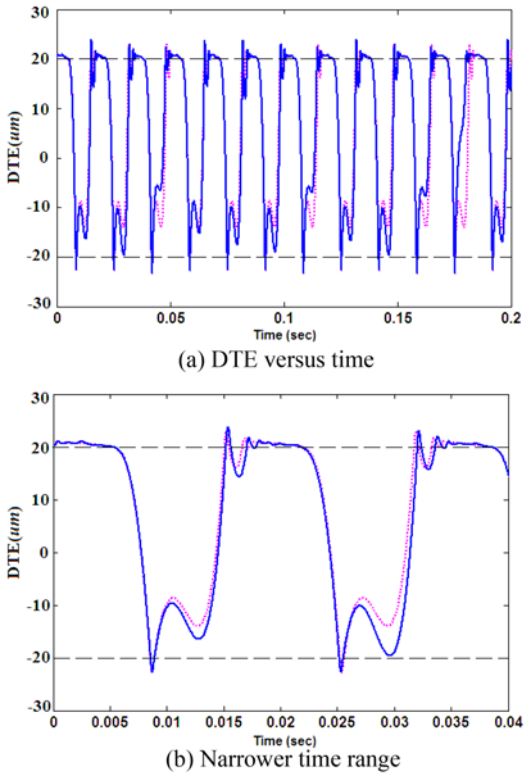

Figure 10. DTE response (A=1000 rad/s^2; f_e=60 Hz; v=1000 rpm; u=0) (Keys: ····· time-invariant meshing stiffness model, ——— time-varying mesh stiffness model developed in Section 2.1).

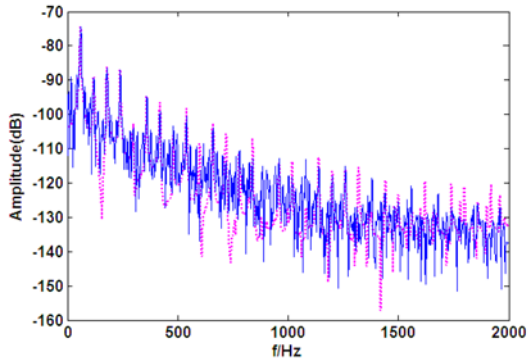

Figure 11. Spectrum of DTE corresponding to the results in Figure 10 (Keys: ····· time-invariant mesh stiffness model, ——— time-varying mesh stiffness model developed in section 2.1).

more significant at higher frequencies. In fact, the temporal variation in the mesh stiffness and its phase shift when the tooth contact switches from one side to the other induces more abundant high frequency components. Additionally, the increase in the input shaft excitation frequency tends to make the impacts more severe and the tooth contact change

direction more frequently. Simultaneously, the number of impacts for the backward tooth contact is reduced to only one in the case of the time-varying mesh stiffness model.

From the results presented above, it can be seen that the time-varying mesh stiffness characteristics for the forward and backward tooth contacts of gears under the idling condition affect the response amplitudes, the time intervals of the impacts and the nature of the spectrum. Higher frequencies tend to be more annoying in the radiated acoustic noise signature. This suggests that the time-varying, asymmetric mesh stiffness should be considered when analyzing the dynamic performance of the idling geared rotor system and that the constant mesh stiffness assumption is not always sufficient, especially when the gear pair is rotating at non-zero mean speeds.

3.3. Effect of Tooth Sliding Friction

The tooth sliding friction, a non-linear and dissipative element, is investigated next to determine its influence on the dynamics of the idling gear pair by applying the proposed dynamic model. The Coulomb friction model applied here is shown in Figure 5. The Coulomb friction model with a periodically varying coefficient of friction $u_i(\theta_p)$ for the i-th meshing tooth pair is derived as follows:

$$u_i(\theta_p) = u \cdot \mathrm{sgn}[mod(\theta_p R_{pb}, \lambda) + (n-i)\lambda - L_{ap}] \quad , i = 0, \ldots, n = \mathrm{floor}(\sigma) \tag{18}$$

where *mod* is the modulus function defined as *mod*(x, y) = x-yfloor(x/y), if y≠0; the floor function rounds off the value in the parentheses to the nearest lower integer; sgn is the sign function; σ is the contact ratio; L_{ap} is the distance between point **a** and **p** in Figure 1(a) and $\boldsymbol{u}$ is the magnitude of the friction coefficient. The friction force on each meshed tooth pair can be calculated from

$$F_{fi} = N_i u_i(\theta_p), i = 0, \ldots, n \, . \tag{19}$$

In the above equation, $\boldsymbol{N}_i$ is the normal contact force acting on the tooth surface.

In this study, the evaluation of the tooth surface friction effect is of interest. The resulting response curves are plotted in Figures 12(b) and 13 in the time and frequency domains, respectively. The DTE response curves shown in Figure 12(a) for friction coefficients of 0, 0.06 and 0.10 coincide well with each other except in the local region shown in Figure 12(b). Figure 13 shows the response spectrum of the DTE from Figure 12. In these results, it can be seen that the tooth sliding friction has very little effect on the response spectrum structure and that all three response spectrum curves coincide quite well with each other. Thus, the tooth sliding friction does not appear to affect the dynamic response of the gear under the idling condition with forward and backward tooth contacts. This appears to be because the friction forces and the resulting moments are much smaller than those caused by the impacts between the gear teeth. Thus, the effect of tooth sliding friction can be neglected.

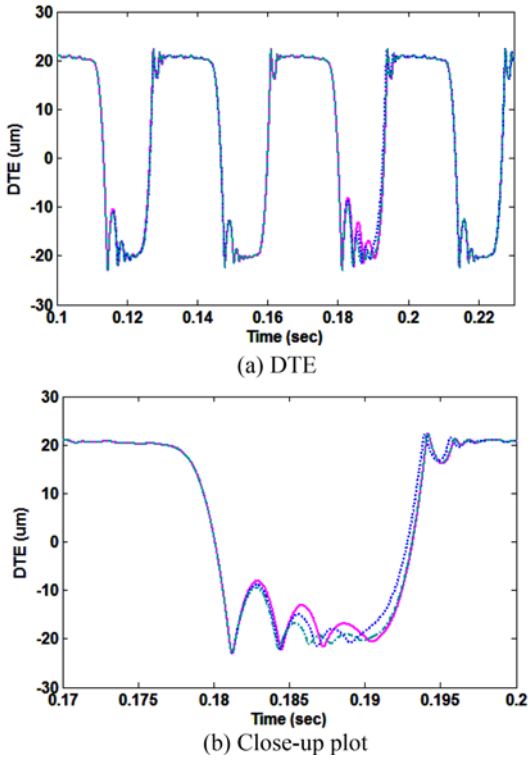

Figure 12. DTE response versus time for different friction coefficients ($\boldsymbol{A}$=1000 rad/s^2, $\boldsymbol{f_e}$=30 Hz, $\boldsymbol{v}$=1000 rpm) (Keys: u=0; u=0.06; u=0.1).

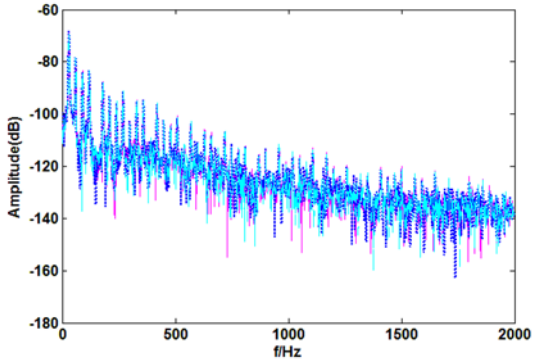

Figure 13. Spectrum of the DTE (unit: m) corresponding to results in Figure 12 (Keys: u=0; u=0.06; u=0.1).

4. CONCLUSIONS

The dynamic response of a gear pair with backlash under the idling condition with drive shaft excitation representing fluctuations in the input load and speed is analyzed. The analysis shows that the gear pair can potentially respond

with both forward and backward tooth contact behaviors. A time-varying mesh stiffness model that incorporates both the forward and backward tooth contact phenomena is developed and used to formulate a six-degree-of-freedom dynamic lumped-parameter gear model representing a spur gear pair system under the idling condition. Comparisons of the results predicted by the time-invariant mesh stiffness model and the proposed time-varying model show clear differences, especially in the higher frequency response components. This can be seen clearly in the frequency domain, where the proposed time-varying, asymmetric mesh stiffness analysis yields additional high frequency effects that are not seen in the time-invariant mesh stiffness model. The differences are more obvious when the gear pair is rotating at the same time. The tooth sliding friction is predicted to have very little effect on the idling gear dynamics. In future work, this proposed time-varying, asymmetric mesh formulation will be applied to the analysis of other kinds of geared transmission systems, like planetary gear systems.

ACKNOWLEDGEMENT–The authors are grateful for the financial support provided by the National Natural Science Key Foundation of China under Contract No. 51035008 and the SKLMT open funds of Chongqing University.

REFERENCES

Brancati, R., Rocca, E. and Russo, R. (2005). A gear rattle model accounting for oil squeeze between the meshing gear teeth. *Proc. Institution of Mechanical Engineers—Part D: J. Automobile Engineering*, **219**, 1075–1083.

Brauer, J. (2005). Transmission error in anti-backlash conical involute gear transmissions: A global–local FE approach. *Finite Elements in Analysis and Design*, **41**, 431–457.

Cai, Y. (1995). Simulation on the rotational vibration of helical gears in consideration of the tooth separation phenomenon (A new stiffness function of helical involute tooth pair). *Trans. ASME, J. Mechanical Design*, **117**, 460–469.

Chaari, F., Fakhfakh, T. and Haddar, M. (2009). Analytical modeling of spur gear tooth crack and influence on gear mesh stiffness. *European J. Mechanics A/Solids*, **28**, 461–468.

Cornell, R. W. (1981). Compliance and stress sensitivity of spur gear teeth. *ASME J. Mech. Des.*, **103**, 447–459.

Crowther, A. R., Singh, R., Zhang, N. and Chapman, C. (2007). Impulsive response of an automatic transmission system with multiple clearances: Formulation, simulation and experiment. *J. Sound and Vibration*, **306**, 444–466.

Dion, J.-L., Moyne, S. L., Chevallier, G. and Sebbah, H. (2009). Gear impacts and idle gear noise: Experimental study and non-linear dynamic model. *Mechanical Systems and Signal Processing*, **23**, 2608–2628.

Dogan, S. N. (1999). Loose part vibration in vehicle transmissions - gear rattle. *Trans. J. Engineering and Environmental Science*, **23**, 439–454.

Fujimoto, T. and Kizuka, T. (2001). An improvement of the prediction method of the idling rattle in manual transmission—in the case of the manual transmission with backlash eliminator. *SAE Paper No.* 2001-01-1164.

Fujimoto, T., Chikatani, Y. and Kojima, J. (1987). Reduction of idling rattle in manual transmission. *SAE Paper No.* 870395.

Han, B. K., Cho, M. K., Kim, C., Lim, C. H. and Kim, J. J. (2009). Prediction of vibrating forces on meshing gears for a gear rattle using a new multi-body dynamic model. *Int. J. Automotive Technology* **10**, **4**, 469–474.

He, S., Cho, S. and Singh, R. (2008). Prediction of dynamic friction forces in spur gears using alternate sliding friction formulations. *J. Sound and Vibration*, **309**, 843–851.

Heinrichs, R. and Bodden, M. (1999). Perceptual and Instrumental Description of the gear rattle phenomenon for diesel vehicles. *6th Int. Cong. Sound and Vibration,* **99**, *Technical University of Demark*, Lyngby.

Houser, D. R. and Harianto, J. (1998). *Load Distribution Program Manual*. The Ohio State University. Columbus. Ohio.

Houser, D. R., Harianto, J. and Ueda, Y. (2004). Determining the source of gear whine noise. *Gear Solutions*, 16–23.

Howard, I., Jia, S. and Wang, J. (2001). The dynamic modelling of a spur gear in mesh including friction and a crack. *Mechanical Systems and Signal Processing* **15**, **5**, 831–853.

Kim, C., Han, B., Cho, M. and Lim, C. (2008). Topology optimization of transmission housings for minimizing the gear rattling noise. *8th World Cong. Computational Mechanics (WCCM8), 5th. European Cong. Computational Methods in Applied Sciences and Engineering (ECCOMAS 2008)*, Venice, Italy.

Kim, T. C. and Singh, R. (2001). Dynamic interactions between loaded and unloaded gear pairs under rattle conditions. *SAE Paper No.* 2001-01-1553.

Luo, A. C. J. and O'Connor, D. (2011). Periodic and chaotic motions in a gear-pair transmission system with impacts. *Nonlinear Science and Complexity*, Part 1, 13–24.

Padmanabhan, C., Rook, T. and Singh, R. (1995). Modelling of automobile gear rattle phenomenon: State of the art. *SAE Paper No.* 951316.

Pimsarn, M. and Kazerounian, K. (2002). Efficient evaluation of spur gear tooth mesh load using pseudo-interference stiffness estimation method. *Mech. Mach. Th.*, **37**, 769–786.

Rebbechi, B., Oswald, F. and Townsend, D. (1996). Measurement of gear tooth dynamic friction. *ASME, DE-, **88**, Proc.* 7th *Power Transmission and Gearing Conf.*, 355–363.

Russo, R., Brancati, R. and Rocca, E. (2009). Experimental investigations about the influence of oil lubricant

between teeth on the gear rattle phenomenon. *J. Sound and Vibration*, **321**, 647–661.

Sarkar, N., Ellis, R. E. and Moore, T. N. (1997). Backlash detection in geared mechanisms: Modelling, simulation and experimentation. *Mechanical Systems and Signal Processing*, **11**, 391–408.

Shih, S., Yruma, J. and Kittredge, P. (2001). Drivetrain noise and vibration troubleshooting. *SAE Paper No.* 2001-01-2809.

Shim, Y., Kauh, S. K. and Ha, K.-P. (2011). Evaluation of idle stability through in-situ torque measurement in automatic transmission vehicles. *Int. J. Automotive Technology* **12**, **3**, 315–320.

Sirichai, S. (1999). *Torsional Properties of Spur Gears in Mesh Using Nonlinear Finite Element Analysis*. Ph.D. Dissertation. Curtin University of Technology.

Tangasawi, O., Theodossiades, S. and Rahnejat, H. (2007). Lightly loaded lubricated impacts: Idle gear rattle. *J. Sound and Vibration*, **308**, 418–430.

Theodossiades, S., Tangasawi, O. and Rahnejat, H. (2007). Gear teeth impacts in hydrodynamic conjunctions promoting idle gear rattle. *J. Sound and Vibration*, **303**, 632–658.

The Ohio State University (1993). *MULTILDP Version 8.22*. Computer Program, Gear Dynamics and Gear Noise Research Laboratory. The Ohio State University. Columbus. Ohio.

Umezawa, K., Suzuki, T. and Sato, T. (1986). Vibration of power transmission helical gears (approximate equation of tooth stiffness). *Bulletin of JSME*, **29**, 1605–1611.

Vaishya, M. and Singh, R. (2001). Analysis of periodically varying gear mesh systems with coulomb friction using floquet theory. *J. Sound and Vibration* **243**, **3**, 525–545.

Walha, L., Fakhfakh, T. and Haddar, M. (2009). Nonlinear dynamics of a two-stage gear system with mesh stiffness uctuation, bearing exibility and backlash. *Mechanism and Machine Theory*, **44**, 1058–1069.

Wang, J. (2003). *Numerical and Experimental Analysis of Spur Gears in Mesh*. Ph.D. Dissertation. Curtin University of Technology.

Wang, M., Manoj, R. and Zhao, W. (2001). Gear rattle modeling and analysis for automotive manual transmissions. *Proc. Institution of Mechanical Engineers—Part D: J. Automobile Engineering*, **215**, 241–258.

Wang, M., Zhao, W., Manoj, R. (2002). Numerical modelling and analysis of automotive transmission rattle. *J. Vibration and Control*, **8**, 921–943.

Weber, C. (1949). *The Deformation of Loaded Gears and the Effect on Their Load-carrying Capacity*. Sponsored Research. British Dept. Sci. and Ind. Res. Report No.3. Germany.

Wu, S., Zuo, M. J. and Parey, A. (2008). Simulation of spur gear dynamics and estimation of fault growth. *J. Sound and Vibration*, **317**, 608–624.

Yakoub, R. Y., Corrado, M., Forcelli, A., Pappalardo, T. and Dutre, S. (2004). Prediction of system-level gear rattle using multibody and vibro-acoustic techniques. *SAE Paper No.* 2004-32-0063.